JOURNAL OF INFORMATION AND COMMUNICATION TECHNOLOGY
https://e-journal.uum.edu.my/index.php/jict

How to cite this article:
Azman, N. F., Jumaat, A. K., Badarul Azam, A. S., Mohd Ghani, N. A. S., Maasar, M. A., Laham, M. F., Nek Abd Rahman, N. (2024). Digital medical images segmentation by active contour model based on the signed pressure force function. *Journal of Information and Communication Technology, 23*(3), 393-419. https://doi.org/10.32890/jict2024.23.3.2

Digital Medical Images Segmentation by Active Contour Model based on the Signed Pressure Force Function

[1]Nor Farihah Azman, [*2]Abdul Kadir Jumaat, [3]Akmal Shafiq Badarul Azam, [4]Noor Ain Syazwani Mohd Ghani,
[5]Mohd Azdi Maasar, [6]Mohamed Faris Laham &
[7]Normahirah Nek Abd Rahman
[1,2&4]School of Mathematical Sciences, College of Computing, Informatics and Mathematics,
Universiti Teknologi MARA, Malaysia
[2]Institute for Big Data Analytics and Artificial Intelligence (IBDAAI), Universiti Teknologi MARA, Malaysia
[3]School of Mathematical Sciences, College of Computing, Informatics and Mathematics, Universiti Teknologi MARA, Sarawak Branch, Mukah Campus, Malaysia
[5]Mathematical Sciences Studies, College of Computing, Informatics and Mathematics, Seremban Campus, Universiti Teknologi MARA (UiTM), Negeri Sembilan Branch, Malaysia.
[6]Institute for Mathematical Research,
Universiti Putra Malaysia, Malaysia
[7]Pusat GENIUS@Pintar Negara, Universiti Kebangsaan Malaysia, Malaysia

[1]farihahazman@uitm.edu.my
[*2]abdulkadir@tmsk.uitm.edu.my
[3]akmalshafiq@uitm.edu.my
[4]syazwanighani@uitm.edu.my

[5] azdimaasar@tmsk.uitm.edu.my
[6] mohdfaris@upm.edu.my
[7] normahirah@ukm.edu.my
*Corresponding author

Received: 19/3/2024 Revised: 8/7/2024 Accepted: 9/7/2024 Published: 28/7 /2024

ABSTRACT

The signed pressure force (SPF) function has recently become a popular function for guiding the curve evolution of the active contour model (ACM) for image segmentation. The aim is to extract the boundaries of digital medical images for shape and image analysis. The recent SPF-based ACM demonstrates effectiveness in image segmentation. However, it may fail if the targeted object is close to a neighbouring object. Additionally, the presence of intensity inhomogeneity and noise in medical images degrades segmentation accuracy and local target areas. Thus, we proposed a new SPF-based ACM, namely the Selective Segmentation with Signed Pressure Force 1 (SSPF1) model, by incorporating the ideas of the SPF function and the distance fitting term based on geometrical constraints. Then, the new SSPF1 model was extended by incorporating an image enhancement technique to develop our second new model, termed the Selective Segmentation with Signed Pressure Force 2 (SSPF2). Numerical results indicated that the SSPF2 model was more recommended than SSPF1 as the SSPF2 model was approximately 4.7% more accurate, as indicated by the Jaccard value and was about 112 times faster in segmenting noisy images compared to the existing selective segmentation model.

Keywords: Active contour model, selective segmentation, signed pressure force function, intensity inhomogeneity, noise.

INTRODUCTION

One of the most challenging tasks in image processing is boundary extraction, also known as image segmentation. The task has grown into an essential part of many image-processing problems. Anter and Abualigah (2023) highlighted the use of image segmentation for liver tumour diagnosis, while Mishra et al. (2022) and Srinivasan et

al. (2023) addressed the task in the application of medical imaging. Other applications included infectious disease (Shewajo & Fante, 2023), shape boundary recognition (Othman et al., 2016) and machine learning (Habeeb et al., 2023). In digital medical image processing, image segmentation is vital in image and shape analysis to extract the boundaries of the medical images by partitioning the entire image area into many distinct sections based on regional consistency.

Due to image equipment, noise, and poor lighting conditions, certain medical images may have noise and intensity inhomogeneity, which refers to the irregularities in the intensity values of a picture that can make it challenging to distinguish between healthy and sick tissue. This can result in medical professionals making erroneous conclusions (Mazlin et al., 2023). Current selective segmentation models deliver unsatisfactory results when segmenting images that are noisy and which suffer from intensity inhomogeneity. Thus, this research aims to address this gap by formulating a new segmentation model to handle images with intensity inhomogeneity and noise.

The segmentation approach can be categorised into two types: global segmentation and selective segmentation. Global segmentation works to segment the entire region of an acquired image. In contrast, the selective segmentation model emphasises segmenting a specific region that must be retrieved (Ghani al., 2022). A variety of image segmentation models have been developed for various reasons (Niu et al., 2017). The most effective global image segmentation algorithms are the learning-based models and the global active contour model (ACM). Learning-based models (machine or deep learning) necessitate a substantial quantity of segmented training images. However, the availability of a large amounts of such images is not always guaranteed.

Compared to learning-based models, the global ACM is less dependent on the amount of data. Additionally, this model has the advantage of being able to cope with topological changes in contour curves. The evolving contour is indicated as the zero-level set in ACM, and is aligned with the object boundaries by reducing the cost function (Caselles et al., 1997; Chan & Vese, 2001; Kass et al., 1988). Global ACMs can be classified into three groups due to the image features used to formulate the energy function: edge-based ACMs (Caselles et al., 1997; Kass et al., 1988), region-based ACMs (Vese & Chan, 2002; Zhu, 1996), and hybrid ACMs (Tian et al., 2013; Zhang et al., 2010).

Edge-based approaches detect object boundaries by using image gradient information to activate a balloon force utilised in curve evolution. For example, the geodesic active contour (GAC) by Caselles et al. (1997) determines the stopping point using an edge-based stopping term and a balloon force term to expand or shrink the contour (Tian et al., 2013). However, the GAC model is unable to detect the target if the image has poor borders, or if the initialisation is too distant from the target's intended object (Li et al., 2015; Soomro et al., 2017). Meanwhile, region-based approaches include statistical information to direct the growing curve toward the true boundary (Cao et al., 2017). As a result, they outperform edge-based ACMs in image segmentation when weak boundaries are present. Among the most prominent region-based ACMs is the Chan-Vese (C-V) model by Chan and Vese (2001), which is founded based on the Mumford Shah (M-S) model by Mumford and Shah (1989). However, when faced with inhomogeneous images, this model is prone to failure. To address this flaw, piece-wise smooth models have been presented, but these models are usually slow due to the intricate procedures required (Tsai et al., 2001; Vese & Chan, 2002).

Hybrid ACMs by Tian et al. (2013) and Zhang et al. (2010) have recently gained prominence among region-based models. In their energy formulations, these approaches consider either region (local intensity or global intensity) and edge information or both local and global intensity information. To segment images effectively, the common function used in formulating hybrid ACMs is the signed pressure force (SPF) function, which can control the segmentation contour's evolution toward the targeted object. Zhang et al. (2010) developed the selective binary and Gaussian filtering regularised level set (SBGFRLS) model, which successfully describes the SPF function theory by integrating components of the GAC and C-V models.

The SPF function can be employed as a comparison centre for obtaining the average intensity values of global inner and outer region-driving centres, causing the contour to expand and contract the inner and outer area of interest. Nevertheless, there exist two main downsides. This begins by iteratively transforming the active contour model by utilising the gradient of the current level, causing it to work excessively slowly. Second, it necessitates the use of a parameter with a considerable impact on the outcomes that can be changed based on the input images.

By employing a novel binary level set formula as well as a novel regularisation operation such as morphological opening and closing, Talu (2013) developed an Online Region-based active contour model (ORACM) that eliminates these two drawbacks. ORACM depends on no parameters and runs faster than traditional ACMs without compromising segmentation accuracy. On top of that, the use of morphological opening and closing together with the SPF function produces a more accurate and smooth segmentation curve.

This study primarily emphasises hybrid-based models due to their potential benefits compared to ACM edge-based and region-based models. Nevertheless, all models mentioned above are global ACMs that aim to segment all objects in each image. A new selective segmentation model is proposed in this paper to accomplish the process of segmenting a specific object.

RELATED WORKS

Selective ACM is used to segment one object of interest from many objects in an image with minimum human input (Ghani et al., 2022). In 2023, a selective ACM based on image saliency was successfully formulated by Mazlin et al. (2023) to segment medical images. The extension of the work in vector-valued medical images was developed by Mazlin et al. (2024). However, both works gave unsatisfactory results in segmenting low-contrast medical images.

Ghani et al. (2022) developed a new selective ACM, named the Primal-Dual Selective Segmentation 2 (PDSS2), with distance function (DF) based on predefined geometrical constraints (marker set) to deal with the issue of segmenting low-contrast images, particularly mammography images. This is accomplished by incorporating the information from image-enhancing techniques, namely histogram stretching. However, this PDSS2 model is incapable of handling images with intensity inhomogeneity and noise.

To overcome the issues of noise and intensity inhomogeneity, Fang et al. (2019) introduced a new hybrid ACM for image segmentation that is driven by weighted global intensity and local intensity region-based SPF named the Weighted Hybrid Region-based Signed Pressure Force (WHSPF) model. The combination of global and local region-based

SPF functions enabled this model to perform global and selective segmentation and develop resiliency toward intensity inhomogeneity and noise. Despite showing a significant improvement over traditional ACMs in segmenting digital medical images, the WHSPF model has a significant drawback in its initialisation, where it requires proper initialisation; otherwise, it may fail if the targeted object is close to another object.

Hence, in this research we aimed to develop a novel selective ACM that can segment digital medical images selectively. The main contributions of the paper are as follows:

- We proposed a novel selective ACM, namely the Selective Segmentation with Signed Pressure Force 1 (SSPF1) model by incorporating the ideas of signed pressure force (SPF) by the WHSPF model and the DF by the PDSS2 model. The ideas allowed the proposed SSPF1 model to effectively handle medical images with intensity inhomogeneity and the presence of noise compared to the WHSPF and PDSS2 models.
- Due to the poor contrast issue of some medical images, the new SSPF1 model was extended by incorporating an image enhancement technique that led to the development of the second new model termed the Selective Segmentation with Signed Pressure Force 2 (SSPF2) model. The ideas allowed the proposed SSPF2 model to handle medical images with intensity inhomogeneity and the presence of noise effectively compared to the WHSPF and PDSS2 models.
- To minimise the computational cost and to obtain a smooth segmentation contour, the Gaussian filtering function and the mathematical morphology operations were proposed to replace the traditional TV regularisation term.
- This research utilised a variety of digital images from different imaging modalities such as ultrasound, mammography, and Magnetic Resonance Imaging (MRI) to enhance the reliability of the research.

The following section of this research presents the research methodology of the proposed model's formulations. Subsequently, the experimental output of both the current and the new models are presented.

THE PROPOSED METHOD

The proposed selective ACMs were discussed in this section by incorporating the ideas of SPF from the WHSPF model by Fang et al. (2019) and DF from the PDSS2 model by Ghani et al. (2022). The description of our SSPF1 and SSPF2 models is given in Figure 1.

Figure 1

Flowchart of the Proposed Model

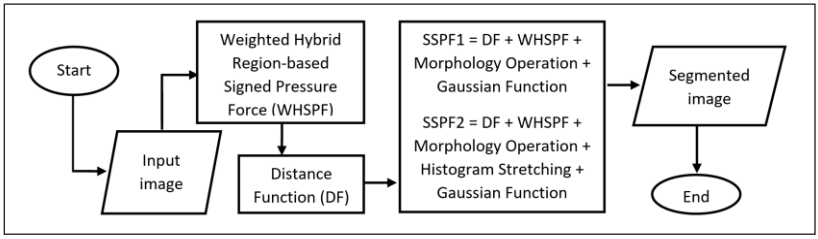

Based on Figure 1, some digital medical images were considered. This was followed by the procedure of obtaining the SPF energy from the WHSPF model and the DF term of an input image. A total energy minimisation function representing the novel SSPF1 model was generated to segment the input image by incorporating the SPF from the WHSPF model and DF energies. Another extension of the new model (SSPF2) was established to discover the effect of image enhancement on segmentation accuracy. Furthermore, the Gaussian function and morphological operations were recommended as regularises in both models instead of the computationally expensive TV term. The following section goes over each of these processes in depth.

Input Image

This study addresses the segmentation of real medical images, including the combination of brain MRI, breast ultrasound, skin disease, and mammography images from diverse sources (Cheng, 2017; Rodtook et al., 2018; Moreira et al., 2012; Codella et al., 2018). The binary ground-truth (benchmark) segmentation for all the test images was obtained from an identical source. The test images had varied levels of intensity inhomogeneity and contained some noise particles to evaluate the ability of the proposed models.

Weighted Hybrid Region-based Signed Pressure Force (WHSPF) Model

Fang et al. (2019) established a new hybrid ACM for image segmentation that is based on SPF derived from weighted global intensity and local intensity areas, namely the Weighted Hybrid Region-based Signed Pressure Force (WHSPF) model. This model can conduct global and selective segmentation due to the integration of global and local region-based SPF functions, namely $spf_{GR}\big(I(x,y)\big)$ and $spf_{LR}\big(I(x,y)\big)$ respectively. The hybrid region-based SPF function $spf_{HR}\big(I(x,y)\big)$ is defined by merging the $spf_{GR}\big(I(x,y)\big)$ and $spf_{LR}\big(I(x,y)\big)$ functions as the following Equation 1:

$$spf_{HR}\big(I(x,y)\big) = w_g \cdot spf_{GR}\big(I(x,y)\big) + w_l \cdot spf_{LR}\big(I(x,y)\big) \qquad (1)$$

where

$$spf_{GR}(I(x)) = I(x) - \frac{w_{g1}(k_1+k_2)(k_1-k_2) + w_{g2}(m+k_2)(m-k_2)}{2(w_{g1}(k_1-k_2) + w_{g2}(m-k_2))}$$

and

$$spf_{LR}\big(I(x)\big) = I(x) - (w_{l1}f_1 + w_{l2}f_2).$$

Here, $I(x)$ is the input image, $w_{g1} = [P_{in}/(P_{in}+P_{out})]$, $w_{g2} = [P_{out}/(P_{in}+P_{out})]$, $w_{l1} = [d_{in}/(d_{in}+d_{out})]$ and $w_{l2} = [d_{out}/(d_{in}+d_{out})]$ where P_{in} and P_{out} are the pixel values of the developing curve's internal and external regions while d_{in} and d_{out} represent the value of local absolute differences inside and outside of the developing curve in the local area.

The constants w_g and w_l are weighted variables employed to balance the impacts of the $spf_{GR}\big(I(x,y)\big)$ and $spf_{LR}\big(I(x,y)\big)$ functions. The constants k_1 and k_2 are the intensity mean within the interior and exterior of the segmentation contour accordingly while m is the inner region's median intensity value. The constants f_1 and f_2 are the

internal and external local region average intensities. The study by Fang et al. (2019) employed an adaptive force propagation function $\alpha\big(I(x,y)\big) = |k_1 + m - 2k_2|$ to adjust the force of the inner and outer sections of the curve, as opposed to the SBGFRLS, with a fixed force. Hence, the model's final level set formulation of WHSPF is defined as the following Equation 2:

$$\frac{\partial \phi}{\partial t} = spf_{HR}\big(I(x,y)\big) \cdot \alpha|\nabla \phi| \tag{2}$$

Based on Equation 2, the function ϕ is the zero-level set segmentation contour with the gradient operator, ∇. The WHSPF model may change the sign of the pressure forces and regulate the propagation of the developing curve indirectly. Alternatively, the contour contracts when it is outside the region of interest (ROI) and extends if it is within the ROI.

Nevertheless, this model is also capable of selective segmentation with proper initialisation. Despite showing a significant improvement over traditional ACMs, the WHSPF model has a significant drawback in initialisation, where this model requires proper initialisation or may fail if the selected region is near another object.

Distance Function (DF)

The Primal-Dual Selective Segmentation 2 (PDSS2) model by Ghani et al. (2022) was successful for the selective segmentation task and was capable of overcoming the problem of segmenting low-contrast images, particularly mammography images. This was carried out by utilising the information from image-enhancing techniques, namely histogram stretching (I_{HS}) for the fitting term, I.

The geometrical constraint (marker set) was implemented in the PDSS2 model and stated as $B = \{w_i = (x_i^*, y_i^*) \in \Omega, 1 \leq i \leq n_1\}$ with $n_1 \geq 3$ marker points must be positioned close to the specified region. The DF defined as $P_d(x,y) = \sqrt{(x - x_g)^2 + (y - y_g)^2}$ represents the

capable of overcoming the problem of segmenting low-contrast images, particularly mammography images. This was carried out by utilising the information from image-enhancing techniques, namely histogram stretching (I_{HS}) for the fitting term, I.

The geometrical constraint (marker set) was implemented in the PDSS2 model and stated as $B = \{w_i = (x_i^*, y_i^*) \in \Omega, 1 \leq i \leq n_1\}$ with $n_1 \geq 3$ marker points must be positioned close to the specified region. The DF defined as $P_d(x, y) = \sqrt{(x - x_g)^2 + (y - y_g)^2}$ represents the Euclidean distance between every point $(x, y) \in \Omega$ from its closest point in the polygon, P such that $(x_g, y_g) \in P$ formed by the user input set, B. Then, the PDSS2 model was constructed as the following Equation 3:

$$\min_{u,w\in[0,1]} PDSS2(u,w), PDSS2(u,w) = \int_\Omega (\mu|\nabla u|_g + [(k_1 - I_{HS})^2 - (k_2 - I_{HS})^2]w + \theta P_d w + \frac{1}{2\rho}(u - w)^2)dxdy \quad (3)$$

In Equation 3, u is the segmentation contour with its dual variable w. The first term is the regularisation term weighted by the parameter μ. The second term is the data fitting term while the third term is the distance term weighted by the parameter θ. The penalty function weighted by ρ is defined in the last term. Based on visual observation, the PDSS2 model can improve test image contrast to disclose detailed information concealed in an image for better segmentation.

However, this model fails to segment images with intensity inhomogeneity and noise since this model uses global average intensity constants (k_1 and k_2) that make it incapable of handling images with intensity inhomogeneity. Furthermore, the first term of Equation 3 which is known as the TV term ($|\nabla u|_g$), is difficult to solve and makes the segmentation process slow.

The Proposed Models

The objective of this research is to establish a model that can effectively and accurately extract the boundary (segment) in digital medical images with inhomogeneous intensity and noise selectively.

Consequently, we introduced a novel selective segmentation model by incorporating the ideas of signed pressure force by the WHSPF model and distance fitting term by the PDSS2 model. Then, the developed SSPF1 model is defined as the following Equation 4:

$$\frac{\partial \phi_{SSPF1}}{\partial t} = (spf_{HR}(I(x,y)) \cdot \alpha - \theta P_d) \cdot \delta_\varepsilon(\phi) \quad (4)$$

Here, α is an adaptive force propagation function, Dirac delta function is denoted by $\delta_\varepsilon(\phi)$ while the distance function is denoted by P_d, weighted by the parameter θ. The function ϕ is the zero-level set segmentation contour. Digital images, especially medical images, are typically characterised by poor contrast which can result in misdiagnosis and inaccuracies.

The segmentation output may be influenced by an image with poor contrast. In an image with good contrast, the intensity values would be evenly distributed across a wide range of intensity values (gray levels). To distribute the intensity values inside a certain range, we can utilise the piecewise linear function, which is defined as the following Equation 5:

$$y = \frac{d-c}{b-a}(x-a) + c \quad (5)$$

Based on Equation 5, the intensity of the output, denoted as *y*, within the range of *c* and *d*, is calculated. Here, *x* represents the input intensity value that falls between the range of *a* and *b* where *a* is set to the lowest 1 percent of *x*, *b* is considered the highest 1 percent of *x* while the values of *c=0* and *d=1* was as recommended by the successful findings presented in the study by Ghani et al. (2022). Equation 5 converts all pixel values below *a* to *c*, and all pixel values above *b* to *d*.

By utilising the concept of redistributing the intensity values by the application of a piecewise linear function described in Equation 5, we introduced an enhanced variant of the SSPF1 model called the SSPF2 model. I_{HS} was denoted as the output of applying Equation 5, thus the SSPF2 is defined as the following Equation 6:

$$\frac{\partial \phi_{SSPF2}}{\partial t} = (spf_{HR}(I_{HS}(x,y)) \cdot \alpha - \theta P_d) \cdot \delta_\varepsilon(\phi) \quad (6)$$

Note that we applied the Dirac delta function $\delta_\varepsilon(\phi) = 1/(\pi\phi^2)$ instead of its approximation $|\nabla\phi|$ as used in the study by Fang et al. (2019). This was to ensure a stable curve evolution can be obtained. To regularise the segmentation contour $\phi(x, y)$ in our proposed SSPF1

and SSPF2 model, we adopted the morphological opening and closing operations and the Gaussian function, $G_\sigma(x,y) = e^{-((x^2+y^2)/2)}$ where σ is the standard deviation. Hence, the updated solution ϕ^{k+1} for SSPF1 and SSPF2 can be written as the following Equation 7 and Equation 8 respectively:

$$\phi^{k+1} = [(\phi^k_{SSPF1} \circ A) \cdot A] * G_\sigma \quad (7)$$

$$\phi^{k+1} = [(\phi^k_{SSPF2} \circ A) \cdot A] * G_\sigma \quad (8)$$

where $*$ is the convolution operator. The structuring element *A* used is a disk type and *k* is the number of iterations in a finite difference scheme environment. This step is important in producing a smooth segmentation curve.

Algorithms to Implement the Proposed Models

The algorithms below demonstrate the procedures required in executing the newly developed models, SSPF1 and SSPF2. In the implementation, MATLAB R2017b software executing at 2.30 GHz and 4 GB of stored memory (RAM) in Intel Core i5-8300H CPU was utilised.

We began with Algorithm 1, which is the SSPF1 model. Once the solution reached the tolerance level, $tol = 0.00001$, or the maximum number of iterations, $maxit = 100$ or $\frac{\|\phi^k - \phi^{k-1}\|}{\|\phi^{k-1}\|} \leq tol$, the iteration process ends. Algorithm 1 for the segmentation process is described further below:

Algorithm 1: Algorithm of the SSPF1 Model

1. Set values of *tol*, *maxit*, σ, w_g, w_l, θ and specify the marker set.
2. Load the input image in MATLAB using 'imread' command.
3. Calculate spf_{HR} based on Equation 1 and compute the DF term, P_d in Equation 3.
4. Define the initial ϕ^0 ($k = 0$) (based on the polygone generated by the marker set.
5. **For** $iter, k = 1$ **do**

Evolve ϕ according to Equation 4 (SSPF1) to obtain ϕ^k.
Regularize ϕ^k using Equation 7.
If $\|\phi^k - \phi^{k-1}\| / \|\phi^{k-1}\| \leq tol$ or *maxit*=100 iterations
end for

6. Otherwise, repeat Step 5 with

Following that, the SSPF2 model is further addressed in Algorithm 2. All steps for the SSPF2 model are identical to the SSPF1 model except in Step 5, where the SSPF2 model solves ϕ iteratively based on Equation 6 and the regularisation process utilises Equation 8. Algorithm 2 for the segmentation process is addressed as follows:

Algorithm 1: Algorithm of the SSPF1 Model

1. Set values of *tol*, *maxit*,σ, w_g, w_l , θ and specify the marker set.
2. Load the input image in MATLAB using 'imread' command.
3. Calculate spf_{HR} based on Equation 1 and compute the DF term, P_d in Equation 3.
4. Define the initial ϕ^0 ($k = 0$)(based on the polygone generated by the marker set.
5. **For** $iter, k = 1$**do**

Evolve ϕ according to Equation 6 (SSPF2) to obtain ϕ^k.
Regularize ϕ^kusing Equation 8.
If $\|\phi^k - \phi^{k-1}\| / \|\phi^{k-1}\| \leq tol$ or *maxit*=100 iterations
end for

6. Otherwise, repeat Step 5 with $k + 1$.

EVALUATION AND RESULTS

Two experiments were conducted to validate the abilities of the proposed models in segmenting medical images with intensity inhomogeneity and noise. The medical images were selected due to their widely recognised characteristic of having non-uniform intensity (intensity inhomogeneity) and noise, which pose challenges in the image segmentation process. The goal of the first experiment is to examine the accuracy and efficiency of our suggested models, namely the SSPF1 and SSPF2 models, in comparison to the WHSPF model by Fang et al. (2019) and the PDSS2 model by Ghani et al. (2022) for the purpose of segmenting real medical images. The second experiment aims to assess the accuracy and efficiency of the proposed SSPF1 and SSPF2 models, in comparison to the WHSPF model and the PDSS2 model, in segmenting real medical images that are contaminated with three types of noise: Speckle, Salt and Pepper, and Gaussian.

In both experiments, the accuracy was assessed using visual observation, Dice (DSC) and Intersection over Union (IoU) also known as Jaccard (JSC) coefficients, as well as the Hausdorff distance (HD). A DSC and JSC value of zero indicates a low level of

segmentation accuracy, whereas a value of one indicates a high level of accuracy. Conversely, a decrease in the HD value corresponds to an increase in segmentation accuracy. Meanwhile, the efficiency was evaluated using time processing (in seconds) by using MATLAB's built-in tic and toc algorithms to obtain a consistent result.

In the subsequent experiments, we set the standard deviation parameter $\sigma = 1.5$, the tolerance $tol = 0.00001$ and the maximum iterations is 100 for all models and images. If the value σ is too small, it is possible to obtain undesirable results, whereas if the value is too large, excessive computation time is required. Next, we set the value of the area parameter θ in the range $\theta = [200,7000]$, the weighted global region-based SPF parameter w_g in the range $w_g = [0.5,60]$ and the weighted local region-based SPF parameter, $w_l = [0.0001,1]$ based on the previous studies of Fang et al. (2019) and Ghani et al. (2022).

Experiment 1: Segmentation on Real Medical Images

Eighteen (18) medical images were employed in the first experiment to verify the ability of the proposed models to selectively segment a targeted object on medical images. The results of the extracted boundary from the segmentation process were compared to the existing WHSPF and PDSS2 models. All the images used were difficult to segment due to their inhomogeneous intensity. The segmentation results used various datasets of medical images, which include brain MRI images by Cheng (2017), breast ultrasound images by Rodtook et al. (2018), and skin lesion images by Codella et al. (2018), as depicted in Figures 2, 3 and 4 respectively.

Figure 2

Segmentation Results on Digital Brain MRI Images

Test Image	WHSPF Model	PDSS2 Model	SSPF1 Model	SSPF2 Model
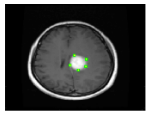	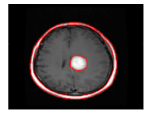	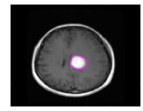	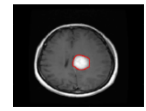	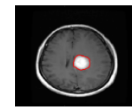
a	b	c	d	e

(continued)

Test Image	WHSPF Model	PDSS2 Model	SSPF1 Model	SSPF2 Model
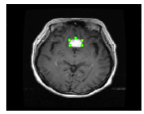	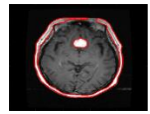	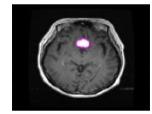	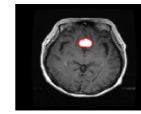	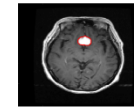
f	g	h	i	j
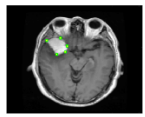	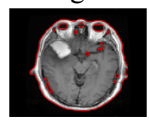	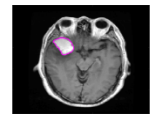	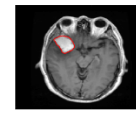	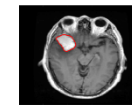
k	l	m	n	o
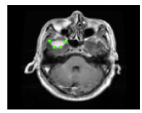	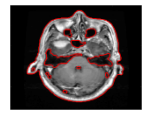	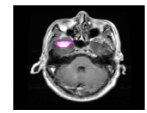	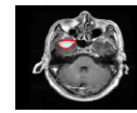	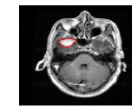
p	q	r	s	t
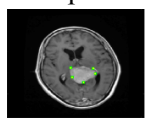	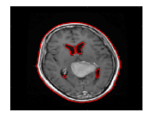	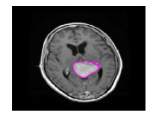	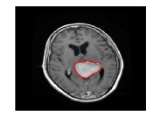	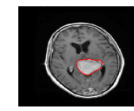
u	v	w	x	y
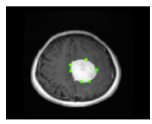	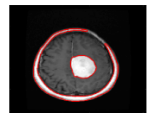	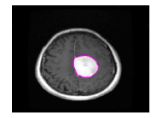	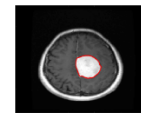	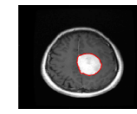
z	aa	ab	ac	ad

Figure 3

Segmentation Results on Digital Breast Ultrasound Images

Test Image	WHSPF Model	PDSS2 Model	SSPF1 Model	SSPF2 Model
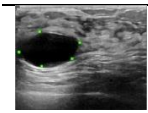	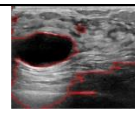	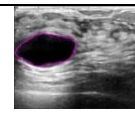	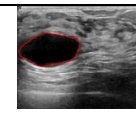	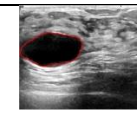
a	b	c	d	e
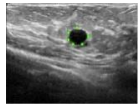	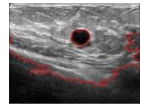	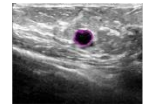	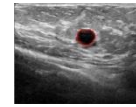	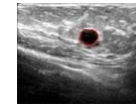
f	g	h	i	j

(continued)

Test Image	WHSPF Model	PDSS2 Model	SSPF1 Model	SSPF2 Model
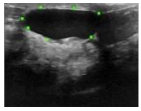	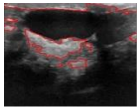	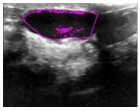	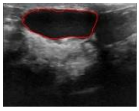	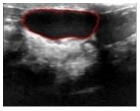
k	l	m	n	o
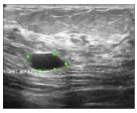	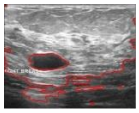	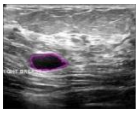	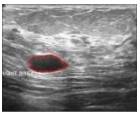	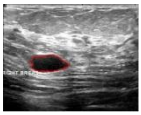
p	q	r	s	t
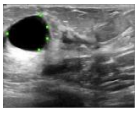	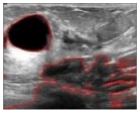	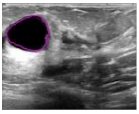	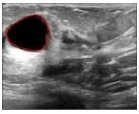	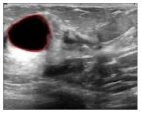
u	v	w	x	y
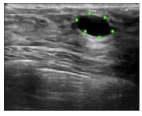	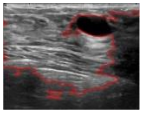	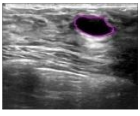	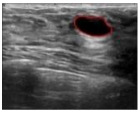	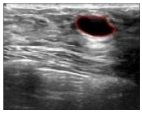
z	aa	ab	ac	ad

Figure 4

Segmentation Results on Digital Skin Lesion Images

Test Image	WHSPF Model	PDSS2 Model	SSPF1 Model	SSPF2 Model
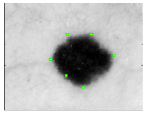	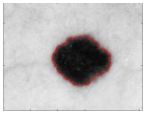	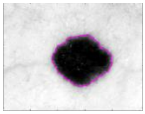	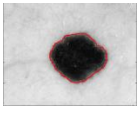	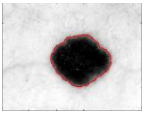
a	b	c	d	e
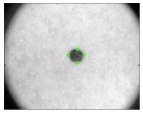	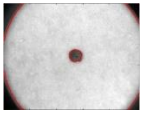	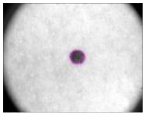	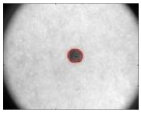	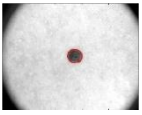
f	g	h	i	j
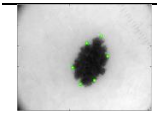	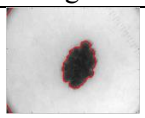	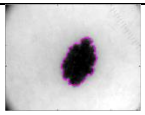	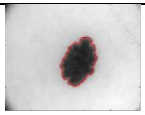	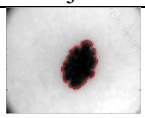
k	l	m	n	o

(continued)

Test Image	WHSPF Model	PDSS2 Model	SSPF1 Model	SSPF2 Model
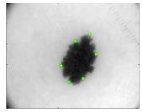	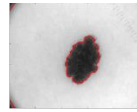	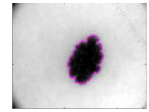	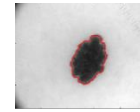	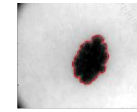
k	l	m	n	o
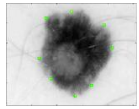	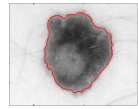	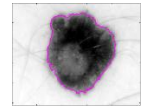	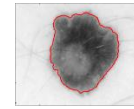	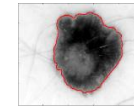
p	q	r	s	t
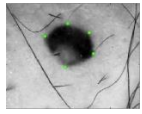	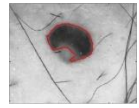	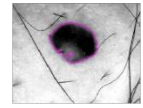	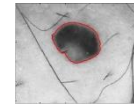	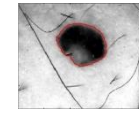
u	v	w	x	y
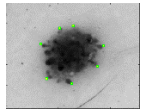	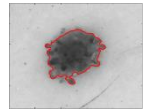	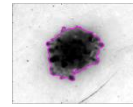	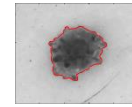	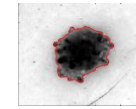
z	aa	ab	ac	ad

As indicated by Figures 2, 3 and 4, the first column displays the image with the marker, denoted by the green markers, to locate the specified object that must be segmented. Additionally, a polygon produced by the markers will serve as the initial contour for all models. Six sample brain images, breast ultrasound images, and skin lesion images are indicated in the first column of Figures 2, 3, and 4, respectively. By visual observation, our proposed models, SSPF1 and SSPF2, and the existing PDSS2 model, were capable of segmenting all the targeted regions in all images compared to the WHSPF model. This was mainly because the SSPF1, SSPF2, and PDSS models were implemented with distance fitting term information which enabled the selective segmentation of the targeted region in the given images effectively.

In addition, the SSPF2 and PDSS2 models can enhance the contrast of the image since these models were formulated using the technique of image enhancement. However, the PDSS2 model segmentation outputs exhibited the presence of noise or artefacts, as highlighted in Figure 3(m) and Figure 3(w). This occurrence can be attributed to the model's limited capability to effectively handle image noise. Our suggested models, SSPF1 and SSPF2 excel at segmenting the noisy

targeted object due to the incorporation of Gaussian function and morphology operators, which effectively smoothen the segmentation contours. On the other hand, the WHSPF model can behave as global segmentation and selective segmentation with proper contour initialisation. However, as shown in the second column of Figures 2 and 3, the WHSPF model is incapable of segmenting the desired object selectively because the aimed object is close to the neighboring object, causing it to have an over-segmentation problem. Nonetheless, due to the local intensity information implemented in this model, the WHSPF can segment images with intensity inhomogeneity.

Besides visual perception, Table 1 tabulates the values of DSC, JSC, HD, and the iteration of the segmentation outcomes for all models.

Table 1

The Values of DSC, JSC, HD, and Iteration for All Test Medical Images for WHSPF, PDSS2, SSPF1 and SSPF2 Models

Medical Image	DSC/JSC/HD/τ/Iterations			
	WHSPF	PDSS2	SSPF1	SSPF2
Brain	0.230/0.143/ 107.056/2.713/11	0.936/0.882/ 3.073/34.882/7	0.954/0.912/ 2.563/2.707/3	0.954/0.913/ 2.563/1.503/3
Ultrasound	0.254/0.152/ 204.100/3.959/38	0.913/0.833/ 7.261/145.167/25	0.932/0.873/ 6.412/3.724/5	0.935/0.878/ 6.080/1.723/6
Skin	0.748/0.647/ 65.397/1.910/6	0.913/0.840/ 7.451/66.482/7	0.915/0.843/ 7.630/1.916/6	0.917/0.847/ 7.395/1.803/6

According to Table 1, the values of DSC, JSC, HD, τ and the iteration for WHSPF, PDSS2, SSPF1 and SSPF2 models are tabulated in the 2nd, 3rd, 4th and 5th columns respectively. A bar chart representing the average values is constructed, as shown in Figure 5, to give the overall insight of the data.

Figure 5

The Average Values of DSC, JSC, HD, and Iteration for all Models

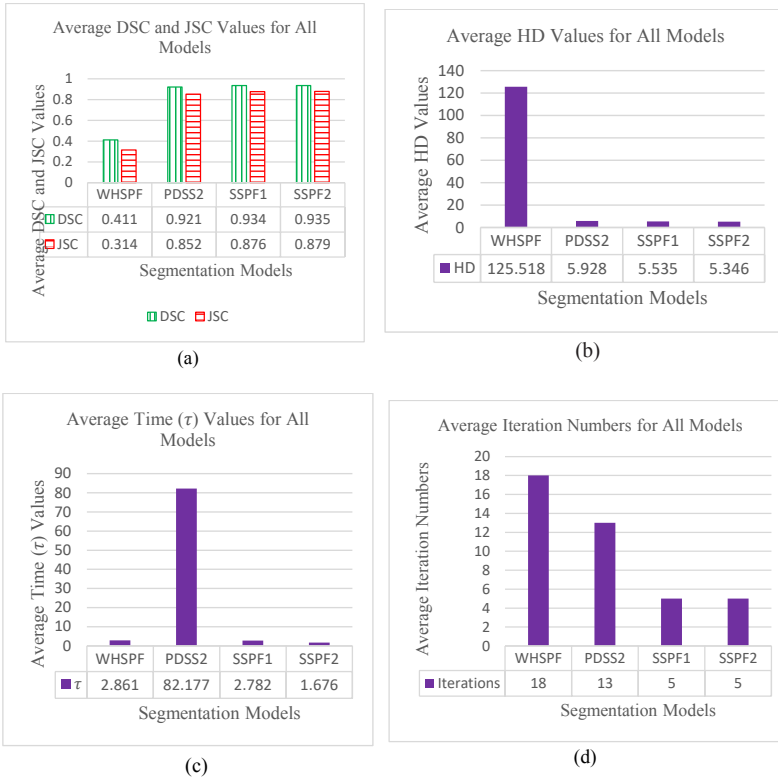

Based on Figure 5(a), the average accuracy values of DSC and JSC for the SSPF2 model gave the highest values with 0.935 and 0.879, respectively, which is 0.1 percent and 0.3 percent higher compared to the SSPF1 model, 1.5 percent and 3.2 percent higher compared to the PDSS2 model, and 127.5 percent and 180 percent higher compared to the WHSPF model. On the other conjunction, our SSPF2 model gave the lowest value of HD as shown in Figure 5(b) with 5.346, which reflects 3.4 percent lower than the SSPF1 model, 9.8 percent lower than the PDSS2 model, and 95.7 percent lower than the WHSPF model. Additionally, based on Figure 5(c) and 5(d), the SSPF2 model gave the lowest values of time processing and iteration with 1.676 seconds and 5 iterations, respectively, which is about 1.6 times faster than the SSPF1 model, 49 times faster than the PDSS2 model, and

1.7 times faster than the WHSPF model. These results indicate that the proposed SSPF2 is superior in efficiency to other models. This is due to the utilisation of the Gaussian function and mathematical morphology operations to regularise the level set formulation in the SSPF2 model, which is more cost-efficient than using the highly computational total variation (TV) function.

Experiment 2: Segmentation of Real Medical Images with Multiple Types of Noise

The goal of Experiment 2 was to testify to the resilience of the proposed models for image segmentation in the existence of noise. There were 3 multiple types of noise, including speckle, salt and pepper, and Gaussian noises. The segmentation results of medical images tainted by these noises are depicted in Figures 6, 7, and 8, respectively.

Figure 6

Segmentation Results on Medical Images with Speckle Noise

Test Image	WHSPF Model	PDSS2 Model	SSPF1 Model	SSPF2 Model
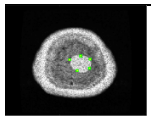	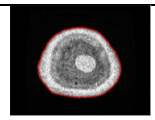	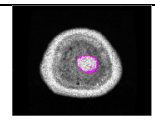	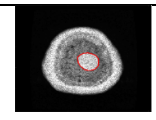	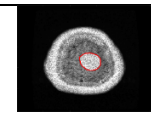
a	b	c	d	e
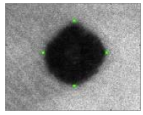	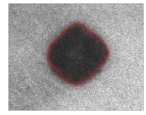	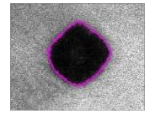	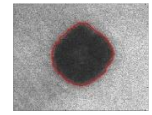	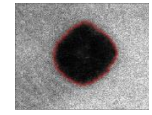
f	g	h	i	j

Figure 7

Segmentation Results on Medical Images with Salt and Pepper Noise

Test Image	WHSPF Model	PDSS2 Model	SSPF1 Model	SSPF2 Model
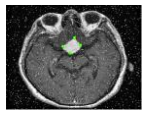	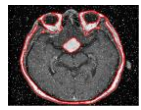	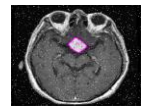	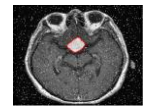	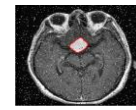
a	b	c	d	e
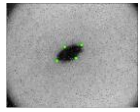	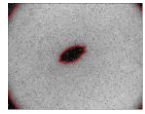	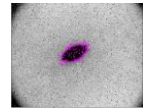	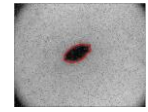	
f	g	h	i	j

Figure 8

Segmentation Results on Medical Images with Gaussian Noise

Test Image	WHSPF Model	PDSS2 Model	SSPF1 Model	SSPF2 Model
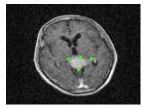	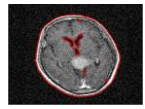	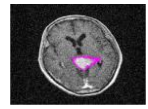	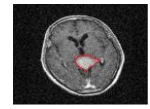	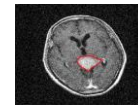
a	b	c	d	e
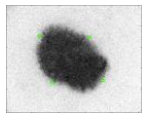	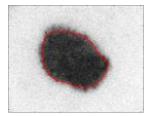	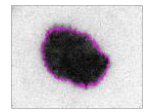	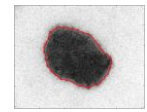	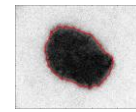
f	g	h	i	j

Figures 6, 7, and 8 demonstrate the segmentation outcomes of the medical images tainted by speckle, salt and pepper, and Gaussian noises, respectively. As illustrated in Figures 6, 7, and 8, our proposed models could produce improved segmentation outcomes in the presence of noise. The WHSPF model was unable to segment the targeted region effectively as the model fails if the targeted object is close to another object, causing it to be unable to segment the aimed regions. Despite this, the WHSPF model was capable of handling images with the presence of noise, while the PDSS2 model generated the worst results when segmenting images with noise. In summary, our

proposed models improved segmentation performance more than the other models for the diversity of medical images with multiple types of noise, as our models were formulated with morphology operations to remove imperfections during segmentation. Table 2 depicts the quantitative results for the accuracy and efficiency of all models as an addition to the visual or qualitative observation.

Table 2

The Values of DSC, JSC, HD, and Iterations for All Test Images with Different Types of Noise for WHSPF, PDSS2, SSPF1 and SSPF2 Models

Medical Image with Noise	DSC/JSC/HD/ τ /Iterations			
	WHSPF	PDSS2	SSPF1	SSPF2
Speckle	0.505/0.434/ 43.378/2.037/6	0.947/0.899/ 3.550/103.948/10	0.957/0.917/ 3.550/3.234/5	0.960/0.923/ 3.916/1.868/4
Salt and Pepper	0.453/0.316/ 150.769/2.520/6	0.933/0.874/ 10.410/495.993/54	0.957/0.917/ 2.414/2.137/5	0.957/0.918/ 2.414/2.089/5
Gaussian	0.469/0.389/ 59.508/4.571/18	0.868/0.768/ 9.853 /100.583/8	0.898/0.815/ 8.550/2.494/5	0.901/0.820/ 8.050/2.309/5

Based on Table 2, the values of DSC, JSC, HD, τ and the iteration for WHSPF, PDSS2, SSPF1 and SSPF2 models are tabulated in the 2nd, 3rd, 4th and 5th columns respectively. Figure 9 displays a bar chart that provides a comprehensive overview of the data by representing the average values.

Figure 9

The Average Values of DSC, JSC, HD, and Iteration for all Models

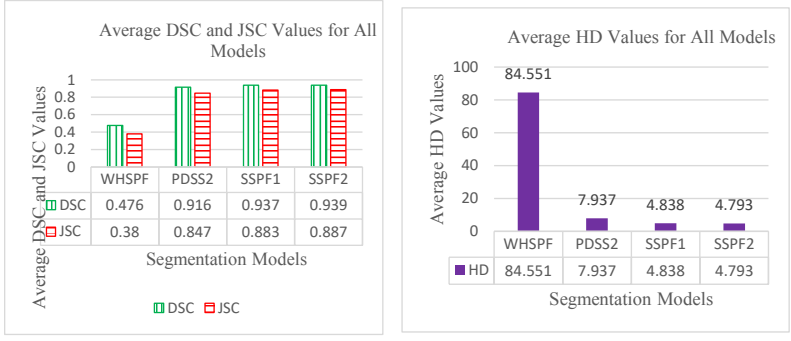

(a) (b)

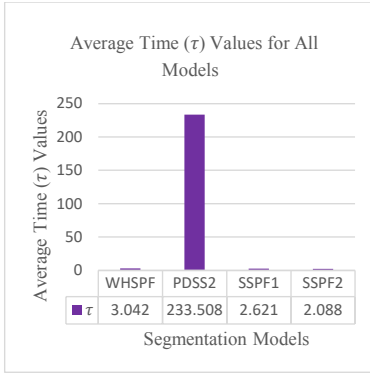

(c)

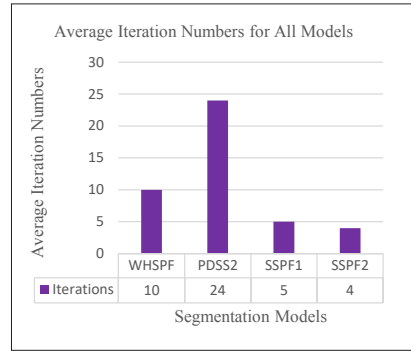

(d)

Based on Figure 9(a), the average accuracy values for the SSPF2 model showed the highest values of DSC and JSC with 0.939 and 0.887, respectively, which is 0.2 percent and 0.5 percent higher compared to the SSPF1 model, 2.5 percent and 4.7 percent higher compared to the PDSS2 model, and 97.3 percent and 133.4 percent higher compared to the WHSPF model. Moreover, based on Figure 9(b), the SSPF2 model had the lowest value of HD with 4.793, which is 0.9 percent lower than the SSPF1 model, 39.6 percent lower than the PDSS2 model, and 94.3 percent lower than the WHSPF model. Meanwhile, based on Figure 9(c) and 9(d), the SSPF2 model's average time processing and iteration numbers indicated the lowest value, which was 2.088 seconds and four iterations, respectively, indicating that this model only required 2.088 seconds to converge, making it the fastest compared to other models which is 1.3 times faster than SSPF1 model, 112 times faster than PDSS2 model, and 1.5 times faster than WHSPF model. Therefore, we may infer that the SSPF2 model could segment the aimed region with a variety of noise faster than the other models in a variety of medical images, where it requires only four iterations to converge accurately.

The results demonstrated that the SSPF2 model can be particularly beneficial in clinical settings where timely analysis is crucial for diagnosis and treatment planning. Additionally, the ability to handle a variety of noise suggests that the model can perform well under different imaging conditions. The model's fast and accurate performance makes it suitable for integration into automated diagnostic systems and artificial intelligence-driven healthcare applications, enhancing the overall capabilities of medical imaging technologies.

CONCLUSION

This research aims to selectively segment a particular region in grayscale medical images with intensity inhomogeneity and noise. Thus, we developed two new models for selective segmentation which are the SSPF1 and SSPF2 models by incorporating the ideas of signed pressure force and distance fitting term, and the SSPF2 model utilises an additional idea of using an image enhancement technique. Furthermore, a Gaussian function and morphological operations were proposed as regularisers to reduce the computational time and remove impurities especially when segmenting images with noise. Numerical experiments revealed that the new SSPF2 model accurately segmented the targeted region in medical images, outperforming previous models. The deficiency of our suggested models is that the parameter values had to be manually established by trial and error to obtain improved outcomes. Manual tuning can lead to inconsistent results as different experts might choose different parameter settings. This variability can affect the reliability and reproducibility of the model's performance. For future work, this research shall be expanded by using a variety of images with different types of structuring elements in morphological operations and by formulating 3-dimensional images for color images. Additionally, an automatic method to determine a suitable parameter for the model can be explored in the future.

ACKNOWLEDGMENT

This work was supported by the Pembiayaan Yuran Penerbitan Artikel (PYPA), Tabung Dana Kecemerlangan Pendidikan (DKP), Universiti Teknologi MARA (UiTM), Malaysia 2024.

REFERENCES

Anter, A. M., & Abualigah, L. (2023). Deep Federated Machine Learning-Based Optimization Methods for Liver Tumor Diagnosis: A Review. *Archives of Computational Methods in Engineering*, *30*(5), 3359-3378. https://doi.org/10.1007/s11831-023-09901-4

Cao, J., & Wu, X. (2017). A novel level set method for image segmentation by combining local and global information. *Journal of Modern Optics*, *64*(21), 2399–2412. https://doi.org/10.1080/09500340.2017.1366564

Caselles, V., Kimmel, R., & Sapiro, G. (1997). Geodesic active contours. *International Journal of Computer Vision*, *22*, 61-79. https://doi.org/https://doi.org/10.1023/A:1007979827043

Chan, T. F., & Vese, L. A. (2001). Active contours without edges. *IEEE Transactions on Image Processing*, *10*(2), 266-277. https://doi.org/10.1109/83.902291

Cheng, J. (2017). Brain tumor dataset (Version 5). Figshare. https://doi.org/10.6084/m9.figshare.1512427.v5

Codella, N. C. F., Gutman, D., Celebi, M. E., Helba, B., Marchetti, M. A., Dusza, S. W., Kalloo, A., Liopyris, K., Mishra, N., Kittler, H., & Halpern, A. (2018). Skin lesion analysis toward melanoma detection: A challenge at the 2017 International symposium on biomedical imaging (ISBI), hosted by the international skin imaging collaboration (ISIC). *Proceedings - International Symposium on Biomedical Imaging*, *2018-April*(Isbi), 168–172. https://doi.org/10.1109/ISBI.2018.8363547

Fang, J., Liu, H., Zhang, L., Liu, J., & Liu, H. (2019). Active Contour Driven by Weighted Hybrid Signed Pressure Force for Image Segmentation. *IEEE Access*, *7*, 97492–97504. https://doi.org/10.1109/ACCESS.2019.2929659

Ghani, N. A. S. M., Jumaat, A. K., & Mahmud, R. (2022). Boundary Extraction of Abnormality Region in Breast Mammography Image using Active Contours. *ESTEEM Academic Journal*, *18*, 115-127.

Habeeb, Z. Q., Vuksanovic, B., & Al-Zaydi, I. Q. (2023). Breast cancer detection using image processing and machine learning. *Journal of Image and Graphics*, *11*(1). https://doi.org/10.18178/joig.11.1.1-8

Kass, M., Witkin, A., & Terzopoulos, D. (1988). Snakes: Active contour models. *International Journal of Computer Vision*, *1*(4), 321-331. https://doi.org/10.1007/BF00133570

Li, X., Jiang, D., Shi, Y., & Li, W. (2015). Segmentation of MR image using local and global region based geodesic model. *BioMedical Engineering Online*, *14*(1), 1–16. https://doi.org/10.1186/1475-925X-14-8

Mazlin, M. S., Jumaat, A. K., & Embong, R. (2023). Saliency-based variational active contour model for image with intensity inhomogeneity. *Indonesian Journal of Electrical Engineering and Computer Science*, *32*(1), 206-215. https://doi.org/10.11591/ijeecs.v32.i1.pp206-215

Mazlin, M. S., Jumaat, A. K., & Embong, R. (2024). Partitioning intensity inhomogeneity colour images via Saliency based active

contour. *International Journal of Electrical and Computer Engineering*, *14*(1), 337-346. https://doi.org/10.11591/ijece.v14i1.pp337-346

Mishra, I., Aravinda, K., Kumar, J. A., Keerthi, C., Shree, R. D., & Srikumar, S. (2022, February). Medical imaging using signal processing: A comprehensive review. In *2022 Second International Conference on Artificial Intelligence and Smart Energy (ICAIS)* (pp. 623-630). IEEE. https://doi.org/10.1109/ICAIS53314.2022.9742778

Moreira, I. C., Amaral, I., Domingues, I., Cardoso, A., Cardoso, M. J., & Cardoso, J. S. (2012). INbreast: Toward a Full-field Digital Mammographic Database. *Academic Radiology*, *19*(2), 236–248. https://doi.org/10.1016/j.acra.2011.09.014

Mumford, D., & Shah, J. (1989). Optimal approximations by piecewise smooth functions and associated variational problems. *Communications on Pure and Applied Mathematics*, *42*(5), 577–685. https://doi.org/10.1002/cpa.3160420503

Niu, S., Chen, Q., De Sisternes, L., Ji, Z., Zhou, Z., & Rubin, D. L. (2017). Robust noise region-based active contour model via local similarity factor for image segmentation. *Pattern Recognition*, *61*, 104-119. https://doi.org/10.1016/j.patcog.2016.07.022

Othman, M., Abdullah, S. L. S., Ahmad, K. A., Bakar, M. N. A., and Mansor, A. R. (2016). The fusion of edge detection and mathematical morphology algorithm for shape boundary recognition. *Journal of Information and Communication Technology*, *15*(1), 133-144. http://e-journal.uum.edu.my/index.php/jict/article/view/8175

Rodtook, A., Kirimasthong, K., Lohitvisate, W., & Makhanov, S. S. (2018). Automatic initialisation of active contours and level set method in ultrasound images of breast abnormalities. *Pattern Recognition*, *79*, 172–182. https://doi.org/10.1016/j.patcog.2018.01.032

Shewajo, F. A., & Fante, K. A. (2023). Tile-based microscopic image processing for malaria screening using a deep learning approach. *BMC Medical Imaging*, *23*(1), 1-14. https://doi.org/10.1186/s12880-023-00993-9

Soomro, S., Akram, F., Munir, A., Lee, C. H., & Choi, K. N. (2017). Segmentation of Left and Right Ventricles in Cardiac MRI Using Active Contours. *Computational and Mathematical Methods in Medicine*, *2017*, 1–16. https://doi.org/10.1155/2017/8350680

Srinivasan, S., Bai, P. S. M., Mathivanan, S. K., Muthukumaran, V., Babu, J. C., & Vilcekova, L. (2023). Grade Classification of Tumors from Brain Magnetic Resonance Images Using a Deep Learning Technique. *Diagnostics*, *13*(6), 1153. https://doi.org/10.3390/diagnostics13061153

Talu, M. F. (2013). ORACM: Online region-based active contour model. *Expert Systems with Applications*, *40*(16), 6233–6240. https://doi.org/10.1016/j.eswa.2013.05.056

Tian, Y., Duan, F., Zhou, M., & Wu, Z. (2013). Active contour model combining region and edge information. *Machine Vision and Applications*, *24*(1), 47–61. https://doi.org/10.1007/s00138-011-0363-7

Tsai, A., Yezzi, A., & Willsky, A. S. (2001). Curve evolution implementation of the Mumford-Shah functional for image segmentation, denoising, interpolation, and magnification. *IEEE Transactions on Image Processing*, *10*(8), 1169–1186. https://doi.org/10.1109/83.935033

Vese, L. A., & Chan, T. F. (2002). A multiphase level set framework for image segmentation using the Mumford and Shah model. *International Journal of Computer Vision*, *50*(3), 271–293. https://doi.org/10.1023/A:1020874308076

Zhang, K., Zhang, L., Song, H., & Zhou, W. (2010). Active contours with selective local or global segmentation: a new formulation and level set method. *Image and Vision computing*, *28*(4), 668-676. https://doi.org/10.1016/j.imavis.2009.10.009

Zhu, S. C. (1996). Region competition: Unifying snakes, region growing, and bayes/mdl for multiband image segmentation. *IEEE Transactions on Pattern Analysis and Machine Intelligence*, *18*(9), 884–900. https://doi.org/10.1109/34.537343